Published in final edited form as:
Biomaterials. 2013 April ; 34(13): 3459–3466. doi:10.1016/j.biomaterials.2013.01.069.

In Vivo Performance of Polymer Nanocarriers Dually-Targeted to Epitopes of the Same or Different Receptors

Iason T. Papademetriou[1], **Carmen Garnacho**[2], **Edward H. Schuchman**[3], and **Silvia Muro**[1,4,*]

[1]Fischell Department of Bioengineering, School of Engineering, University of Maryland, College Park, MD 20742, USA

[2]Department of Cytology and Histology, Faculty of Medicine, University of Seville, Seville, Spain

[3]Department of Human Genetics, Mount Sinai School of Medicine, New York, NY 10029, USA

[4]Institute for Bioscience and Biotechnology Research, University of Maryland, College Park, MD 20742, USA

Abstract

Modification of drug delivery nanomaterials with affinity molecules that facilitate targeting, has rendered a new class of ligands for cell receptors, which often possess valency and dimensions different from natural counterparts. Designing strategies to target multiple receptors or, never explored, multiple epitopes on the same receptor may modulate the biodistribution properties of these nanomaterials. We examined this using antibody-directed targeting of polymer nanocarriers to transferrin receptor (TfR) and intercellular adhesion molecule 1 (ICAM-1). Regarding epitopes on one receptor, nanocarriers addressed with anti-TfR-R17 maintained brain and lung targeting in mice, compared with “free” antibody, while anti-TfR-8D3 nanocarriers lost specificity. Coating nanocarriers with both antibodies decreased targeting in brain and liver, not lungs, modulating biodistribution. Regarding different receptors, nanocarriers coated with both anti-ICAM and anti-TfR displayed intermediate specific accumulation in lungs and higher in liver, compared to single-targeted nanocarriers, while brain targeting was comparable to TfR- and lower than ICAM-1-targeted nanocarriers. Tracing a model therapeutic cargo, acid sphingomyelinase (enzyme replacement for Niemann-Pick Disease A-B), showed that combined-targeted anti-ICAM/TfR nanocarriers enhanced enzyme delivery versus “free” enzyme, with biodistribution patterns different from single-targeted nanocarriers. Hence, targeting nanocarriers to multiple epitopes or receptors holds promise to control distribution of drug delivery nanomaterials in the body.

1. Introduction

The ability to design nanomaterials with controllable composition, architecture, and functionalities has greatly impacted the field of drug delivery and holds considerable promise to improve clinical interventions [1]. An important aspect of design of such nanomaterials is that of conferring them active targeting properties, so that the therapeutic agents they carry can reach the intended site in the body to exert the desired effect. For this

*Address correspondence to Silvia Muro, Institute for Bioscience & Biotechnology Research, 5115 Plant Sciences Building, College Park, MD 20742, US; Phone: 1-301-405-4777; Fax: 1-301-314-9075; muro@umd.edu.

purpose, the surface of drug nanocarriers can be modified with targeting moieties (antibodies, peptides, *etc.*) addressed to receptors expressed on specific tissues and cells [2]. If these receptors have endocytic capacity, targeting can then enable transport into cells or across cellular barriers [3–5]. While most natural ligands in the body represent relatively small, mono or divalent, soluble molecules, targeted nano-scaled drug delivery systems represent, for the most part, new types of ligands which display high multivalency and size within a few dozens-to-hundreds of nanometers [6].

Moreover, nanomaterials for drug delivery can be modified to achieve combined-targeting or binding to more than one cell-surface marker. In nature, this phenomenon is observed in mammalian systems in the case of infectious pathogens and immune system functions [7, 8], while most ligands (metabolites, vitamins, carrier proteins, hormones, neurotransmitters, *etc.*) bind only to one receptor. However, this approach holds potential in drug delivery, since most markers are not exclusively expressed in a precise site *in vivo,* and high affinity of targeted nanocarriers may lead to non-desired accumulation in regions of the body associated with low expression [6]. Hence, targeting drug nanocarriers to multiple receptors could help modulate biodistribution. An example is that of systems addressed to multiple cell adhesion molecules, which improve endothelial anchoring [9–12]. Similar strategies have shown improved detection of vulnerable atherosclerotic plaques, inflammation, enhanced brain glioma therapy, or facilitated targeting and transport to the brain [13–16]. However, this approach is still relatively unexplored, particularly in the context of targeting receptors with disparate function or associated with different endocytic pathways.

In addition, an intriguing strategy is that of directing nanocarriers to multiple epitopes of the same receptor. Although this has never been tested, stimulation of a receptor at one epitope is known to alter activity at another epitope. Such is the case for stimulation *in vivo* of platelet-endothelial cell adhesion molecule 1 (PECAM-1) with an antibody, which subsequently enhanced lung accumulation of a second antibody or fusion conjugate [17]. Binding, endocytosis, and lysosomal transport of PECAM-1-targeted nanocarriers were shown to depend on the epitope targeted [18]. Epitope selection is important for lung accumulation and induced cleavage of anti-angiotensin converting enzyme [19, 20], and brain selectivity of anti-transferrin receptor (TfR) [21]. Therefore, epitope-dependent targeting merits further investigation.

In this study, we explored the impact of dual-targeting to different epitopes of the same cell-surface receptor or different receptors in terms of *in vivo* biodistribution of model polymer nanocarriers. We focused on targeting TfR and/or intercellular adhesion molecule 1 (ICAM-1), for which extensive previous studies exist [22–32]. TfR is expressed on various tissues, including the blood-brain barrier and cancer, and functions in iron transport [33, 34]. ICAM-1 is expressed primarily on endothelium (including peripheral organs and brain) and other cell types, functions in leukocyte adhesion and transmigration, and is over-expressed in many pathologies [35, 36]. Although through different pathways (clathrin- versus cell adhesion molecule-mediated transport [31, 34]), ligands to TfR or ICAM-1 provide drug targeting, as well as intra- and trans-cellular transport of drugs and their carriers in cell culture and animal models [4, 22, 23, 37], highlighting the relevance of these receptors in the context of drug delivery.

2. Materials and Methods

2.1. Antibodies and Reagents

Monoclonal antibody against mouse ICAM-1 was YN1 (anti-ICAM). Monoclonal antibodies against mouse TfR were clone R17217 (anti-TfR-R17) from Biolegend (San Diego, CA) and clone 8D3 (anti-TfR-8D3) from Novus Biologicals (Littleton, CO). Non-

specific IgG was from Jackson immunoresearch (Pike West Grove, PA). Recombinant human acid sphingomyelinase (ASM) was produced and purified as described [38]. Polystyrene particles (100 nm diameter) were from Polysciences (Warrington, PA). Iodogen was from Thermo Fisher Scientific (Waltham, MA). Unless otherwise stated, all other reagents were from Sigma Chemical (St. Louis, MO).

2.2. Preparation and characterization of nanocarriers targeted to ICAM-1 or TfR

Model targeted polymer nanocarriers were prepared by coating ^{125}I-labeled antibodies or a mix of antibodies and ^{125}I-labeled ASM enzyme (50:50 mass ratio) on 100 nm polystyrene nanoparticles *via* surface adsorption, as described [39]. Regarding the antibody component: (a) non-specific nanocarriers contained only control IgG; (b) nanocarriers targeted to different epitopes of the same receptor displayed anti-TfR-R17 and/or anti-TfR-8D3, or combinations of either one of these antibodies and IgG; and (c) nanocarriers targeted to different receptors displayed anti-TfR-R17 and/or anti-ICAM, or combinations of either one of these antibodies and IgG. Where two antibodies were coated on the same nanocarrier, a 50:50 molar ratio was used. Uncoated counterparts were removed by centrifugation. Nanocarriers were then resuspended in phosphate-buffered saline containing 0.3% bovine serum albumin and sonicated, to avoid aggregation. The final size and zeta potential of nanocarrier formulations were estimated by dynamic light scattering (Malvern Zetasizer, Worcestershire, UK). The antibody coating density was assessed by measuring ^{125}I content in a gamma counter (PerkinElmer Wizard$_2$Waltham, MA). The characterization of the formulations used is summarized in Table 1.

2.3. Binding of antibodies or antibody-coated nanocarriers to cells in culture

Mouse heart endothelial cells (H5V) [40] were seeded on gelatin-coated coverslips, and cultured at 37°C, 5% CO2, and 95% relative humidity in DMEM medium supplemented with 10% fetal bovine serum, 2 mM glutamine, 100 u/ml penicillin, and 100 μg/ml streptomycin. After reaching confluency, cells were incubated at 37°C for 1 hour with free anti-ICAM, anti-TfR-8D3, anti-TfR-R17, or control IgG, or with FITC-labeled nanocarriers coated with either one or dual combinations of these antibodies, as described above. After removing unbound materials, cells were fixed with 2% paraformaldehyde, and permeabilized with 0.2% Triton X-100 to allow detection of internalized free antibodies. Free antibodies were visualized by staining with FITC-labeled goat anti-mouse IgG, while antibody-coated carriers required no additional staining since FITC is contained within the polymer matrix. Fluorescence microscopy images were taken using an Olympus IX81 microscope (Olympus, Inc., Center Valley, PA), ORCA-ER camera (Hamamatsu, Bridgewater, New Jersey), 60x objective (Olympus Uplan F LN; Olympus) and FITC-optimized filter (3540B-OMF; Semrock, Inc., Rochester, NY). Images were acquired with SlideBook 4.2 (Intelligent Imaging Innovations, Denver, Colorado), and analyzed using Image-Pro 6.3 (Media Cybernetics, Inc., Bethesda, MD) to estimate antibody presence by mean fluorescence intensity, or carriers associated per cell by counting the number of fluorescent objects. This binding characterization is also summarized in Table 1.

2.4. Biodistribution and therapeutic enzyme targeting by antibodies or antibody-coated nanocarriers

Mice used in this study were C57BL/6J males, either control or challenged intraperitoneally with 1 mg/kg bacterial lipopolysaccharide 24 h prior to experiments, to mimic pathological inflammation, then anesthetized for the following i.v. injections. A group of mice was injected with free antibodies (^{125}I-labeled anti-ICAM, anti-TfR R17 or 8D3, or IgG; ~1.3 mg antibody/kg) or ^{125}I-ASM (~0.7 mg ASM/kg). Another set of mice was injected with nanocarriers coated with either one or a mix of two antibodies, as per Table 1 (~1.3 mg antibody/kg, ~1.8×10^{13} particles/kg). A final group of mice was injected with a mix of one

or two targeting antibodies and ^{125}I-ASM (~0.7 mg ASM/kg, ~1.8×10^{13} particles/kg), described above. Organs representative of the central nervous system, peripheral tissue, and the reticulo-endothelial system (brain, lungs, and liver, respectively) were harvested following euthanasia at 30 min post-injection. The ^{125}I content and weight of the samples were determined to estimate the organ-to-blood localization ratio (LR) and specificity index (SI) of the formulations. LR is the percent of injected dose accumulated per gram of tissue (%ID/g) divided by the %ID/g of blood, which normalizes biodistribution to account for differences in organ size and blood fraction [41]. The SI is calculated as the LR of targeted formulations divided by the LR of non-targeted counterparts, and represents the specific targeting to an organ [41]. These studies were carried out in accordance with IACUC and University of Maryland regulations.

2.5. Statistics

Data were calculated as mean ± standard deviation of the mean (S.E.M.), where statistical significance was determined as $p<0.05$ by Student's *t*-test.

3. Results and Discussion

3.1. Biodistribution of antibodies and antibody-coated nanocarriers targeted to TfR

Since multivalency and size of targeted nanocarriers differ from that of naked targeting moieties, we first examined the targeting pattern of two distinct anti-TfR antibodies, clone 8D3 versus R17217 (abbreviated R17). Specific targeting of these antibodies was verified using endothelial cells in culture and compared to non-specific IgG (data not shown), verifying previously reported results [21]. Then, these antibodies were injected i.v. as free ^{125}I-labeled counterparts in mice to assess their *in vivo* biodistribution. We focused on brain, lungs, and liver as examples of central nervous system, peripheral, and clearance organs, respectively.

Figure 1 shows the localization ratio (LR) and specificity index (SI) of these antibodies, which represent the organ-to-blood ratio normalized per weight of these tissues, and the corresponding specific organ accumulation as compared to control IgG (see Methods). Both anti-TfR-8D3 or anti-TfR-R17 resulted in comparable (Figure 1A) and specific accumulation in brain (SI value above 1; Figure 1B), yet they also accumulated considerably and specifically in other organs. Anti-TfR-8D3 targeted TfR throughout the body more efficiently than anti-TfR-R17, yet the specificity of this antibody in peripheral organs exceeded its brain specificity, which was not observed in the case of anti-TfR-R17. This is despite the fact that both antibodies display similar affinity [23, 42], and in agreement with greater targeting of anti-TfR-8D3 in cell culture (1.5±0.09-fold over anti-TfR-R17 staining; $p<0.001$; data not shown). This result is also consistent with previous work showing the different biodistribution patterns of these antibodies *in vivo* 21], which may be due to differential accessibility of their respective epitope targets, or different presence through the body of receptor isoforms predominantly exposing these particular epitopes. Indeed, previous works have shown difference in reactivity of anti-TfR antibodies to different cell lines or tissues *in vivo* 43, 44], and two TfR isoforms displaying distinct post-translational glycosylations have been reported in mice [45].

Next, we assessed targeting of nanocarriers coated with anti-TfR-8D3 or anti-TfR-R17. As in our previous studies and in order to avoid potential confounding results of concomitant nanoparticle degradation, we used model polystyrene nanoparticles which, after antibody coating, have shown similar targeting and biodistribution to biodegradable poly(lactic-co-glycolic acid) counterparts [46] and, hence, represent a valid model. Nanocarriers coated with anti-TfR-R17 or anti-TfR-8D3 had similar characteristics, with size ranging between

~235–265 nm, zeta potential from −14.5 to −16 mV, and coating density of 185–220 antibody molecules per particle , and they both showed specific targeting to endothelial cell cultures (Table 1).

Nanocarriers coated with anti-TfR-R17 or anti-TfR-8D3 both displayed increased accumulation in brain, lungs, and liver in comparison to their free antibody counterparts (Figures 2A and 3A). This result pairs well with enhanced avidity of nanocarriers due to high valency and also indicates a different biodistribution pattern, as in the case of free antibodies. Although brain still showed specific uptake for both types of nanocarriers (SI > 1), surprisingly, the targeting specificity of anti-TfR-8D3 nanocarriers over control IgG nanocarriers was decreased in lungs, liver, and slightly in brain in comparison to that of free anti-TfR-8D3 (Figure 2B). This was in contrast to anti TfR-R17 nanocarriers, which displayed only decreased specificity toward the liver, but not the brain or lungs (Figure 3B).

Therefore, it appears that enhanced organ uptake of nanocarriers may be in part due to nonspecific accumulation. This is in accord to our recent work showing that, despite enhanced valency, anti-TfR nanocarriers pose steric hindrances leading to poor binding and suboptimal induction of endocytosis as compared to free antibodies, according to TfR length and natural size restrictions of clathrin-coated pits [39]. In this situation, it is possible that anti-TfR nanocarriers may bind non-specifically to Fc receptors in tissues, resulting in low specificity. Also, this effect seems to depend on the precise epitope targeted and, consequently, its different location and accessibility.

In general, anti-TfR-R17 nanocarriers displayed more robust targeting vs anti-TfR-8D3 counterparts, as opposed to free antibodies. A similar outcome has been observed for nanocarriers addressed to different epitopes of PECAM-1, where targeting to membrane proximal epitopes resulted in lack of nanocarrier targeting [18]. This highlights the rather overlooked relevance of precise epitope targeting, and its implications in designing effective targeted drug delivery systems. Greater targeting by anti-TfR-R17 nanocarriers *in vivo* is opposite to greater targeting by anti-TfR-8D3 nanocarriers in cell culture (Table 1), also emphasizing differences on the presence and accessibility of their corresponding epitopes in different cell types and tissues [21, 43–45]

3.2. Biodistribution of nanocarriers dually-targeted to two distinct TfR epitopes

We next examined the biodistribution behavior of nanocarriers coated with both anti-TfR-8D3 and anti-TfR-R17 (anti-TfR-R17/8D3 nanocarriers). This is, to the best of our understanding, the first time that dual-targeting to epitopes on the same receptor is examined. These nanocarriers displayed similar size, zeta potential, and total antibody surface-coating than single-targeted counterparts (with a 50:50 coating-ratio of anti-TfR-R17-to-anti-TfR-8D3), and bound specifically to endothelial cells in culture (Table 1).

As compared to either parent nanocarrier, dually-targeted anti-TfR-R17/8D3 counterparts displayed reduced accumulation in brain and comparable pulmonary levels, while liver accumulation was similar to that of anti-TfR-8D3 nanocarriers and lower than for anti-TfR-R17 counterparts (Figure 4A). In addition, anti-TfR-R17/8D3 nanocarriers lost targeting specificity for all three organs, as their SI value fell below 1 (Figure 4B). These effects could in theory be explained by reduced overall avidity of dually-targeted nanocarriers toward each independent epitope on TfR. Indeed, the specificity of anti-TfR-R17/8D3 in liver and lung had an intermediate value compared to that of single-targeted nanocarriers coated at similar valencies (anti-TfR-R17/IgG and anti-TfR-8D3/IgG; Figure 4). However, this was not the case for brain, where dually-targeted nanocarriers accumulated below the level of both anti-TfR/IgG counterparts. It is possible that binding to two TfR epitopes may modify the conformation of the receptor so that exposure and, hence, binding to these

epitopes may become impaired, displacing the antigen antibody equilibrium toward the unbound form. Conceivable, this phenomenon could impact firm binding of dually-targeted nanocarriers at different extents in tissues expressing different receptor isoforms [43, 44], such as those displaying different post-translational glycosylations [45]. However, at present, the distribution of these TfR glycoforms in brain vs. other organs remains uncharacterized.

Interestingly, it appears that biodistribution of dually-targeted nanocarriers depended more on the epitope targeted by anti-TfR-8D3 vs anti-TfR-R17. For instance, 50% reduction in valency did not impact targeting or specificity by anti-TfR-R17 (anti-TfR-R17 vs anti-TfR-R17/IgG nanocarriers), while a similar reduction negatively impacted both parameters in the case of anti-TfR-8D3 (anti-TfR-8D3 vs anti-TfR-8D3/IgG nanocarriers). A 50% reduction in valency also decreased targeting to the anti-TfR 8D3 epitope in cell culture, while targeting to the anti-TfR-R17 epitope showed a slight, yet statistically significant, improvement (see Table 1). This type of result highlights, once more, the role of precise epitope targeting in drug delivery, the dependency on cell and tissue type (apart from other factors), and the unpredictability of these outcomes, yet indicating for the first time that combined targeting to multiple epitopes of a single cell-surface receptor may help modify the biodistribution of nanomedicines.

3.3. Biodistribution of nanocarriers dually-targeted to TfR and ICAM-1

We then examined combination-targeting toward different receptors. Although this approach has been explored previously, most prior strategies aimed at targeting receptors of similar type or function, such as endothelial cell adhesion molecules involved in leukocyte adhesion and extravasation [9–14], or receptors involved in similar endocytic transport pathways, particularly regulated *via* clathrin-coated pits [15, 16, 47–51]. Only in a couple of examples, the receptors targeted associated with different endocytic mechanisms, yet these targeting studies did not assess targeting *in vivo* 52, 53]. We focused on targeting receptors of unrelated function, regulation, and endocytic mechanism: TfR and ICAM-1, involved in iron transport vs. leukocyte transmigration, which display unmodified vs. up-regulated expression under inflammatory mediators, and transport materials *via* clathrin vs. CAM endocytosis, respectively [22, 36]. As shown in Table 1, nanocarriers coated with both anti-ICAM and anti-TfR clone R17 (anti-ICAM/TfR) displayed size, zeta potential, and total antibody surface-coating similar to their single-targeted counterparts, with a 50:50 coating-ratio of anti-ICAM to anti-TfR. These nanocarriers also targeted specifically endothelial cells in culture, as compared to control IgG-coated nanocarriers (Table 1).

As in our recent work [39] and in accord with greater targeting of nanocarriers to ICAM-1 in cell cultures (Table 1), anti-ICAM nanocarriers had greater accumulation and targeting specificity than anti-TfR nanocarriers in the brain and lungs, with similar liver uptake (Figure 5). Nanocarriers targeted to both ICAM-1 and TfR displayed lung accumulation and specificity which was intermediate of parental formulations, similar to the outcome observed in cell culture (Figure 5 and Table 1). This may be due to reduced valency of dually-targeted nanocarriers toward anti-ICAM, since control anti-ICAM/IgG nanocarriers had a similarly reduced pulmonary uptake and reduced targeting in cell culture (Figure 5 and Table 1). However, although lower, pulmonary uptake *via* anti-TfR was not affected by decreasing valency of this component (compare anti-TfR and anti-TfR/IgG nanocarriers). This suggests a stronger dependency on antibody surface-density for ICAM-1 vs. TfR targeting, in agreement with our previous work showing that multivalency associated with nanocarriers vs. free antibodies, enhances specific targeting and endocytosis toward ICAM-1, while an opposite effect is observed for TfR [39].

Interestingly, brain accumulation and specificity of dually-targeted anti-ICAM/TfR nanocarriers were comparable to anti-TfR nanocarriers and lower than anti-ICAM counterparts (Figure 5). This was independent of valency changes toward anti-ICAM or anti-TfR, since brain uptake of anti-ICAM/IgG or anti-TfR/IgG nanocarriers was similar to their parental single-targeted counterparts. Anti-TfR vs. anti-ICAM ruled brain targeting, despite the fact that anti-ICAM nanocarriers accumulate in brain better. In a previous work, we observed reduced endocytosis of nanocarriers *via* TfR compared to free antibodies, while the opposite scenario arose for ICAM-1 targeting [39]. Therefore, it is possible that binding of anti-ICAM/TfR nanocarriers to TfR reduces or delays uptake by cells despite the presence of anti-ICAM, lowering brain accumulation. This was not observed in lungs, likely due to relatively high ICAM-1 expression in this organ vs. the brain [41, 54]. Liver uptake of anti-ICAM/TfR nanocarriers behaved differently, which was slightly greater compared to parent single-targeted formulations. This may be due to reduced accumulation of these particles in the lungs, and may also possibly represent increased targeting since liver displays both specific accumulation (due to ICAM-1 and TfR expression) as well as non-specific clearance.

3.4. Biodistribution of a therapeutic cargo, ASM enzyme, by nanocarriers dually-targeted to TfR and ICAM-1

The data shown above support that exploiting different expression, valency requirements, and mechanistic patterns associated with distinct cell-surface receptors *via* multiple-targeting, holds potential to modify the biodistribution of drug delivery systems. We examined the impact of this approach on the delivery of a model cargo, recombinant acid sphingomyelinase (ASM), a lysosomal enzyme deficient in genetic Niemann-Pick disease A-B [38]. ASM is currently explored for enzyme replacement therapy by i.v. injection of the naked enzyme. In this case, delivery is necessary both in the brain and peripheral organs, including primarily the lungs and reticulo-endothelial system, typically affected in this disease [38].

As in our recent work [39], coupling ASM to either anti-ICAM or anti-TfR nanocarriers significantly enhanced accumulation level and specificity of ASM targeting in the brain, lungs and liver in comparison to injection of the free enzyme, with a greater improvement in the case of anti-ICAM nanocarriers (Figure 6). Dually-targeted anti-ICAM/TfR nanocarriers also resulted in enhanced ASM accumulation and specificity in all three organs compared to free enzyme. In comparison to single-targeted counterparts, this formulation displayed intermediate values of ASM accumulation and specificity in the lung, and values more similar to those corresponding to ASM delivery by anti-TfR nanocarriers in the brain and liver. This is similar to the result observed when tracing anti-ICAM/TfR nanocarriers (Figure 5), showing paired co-distribution of the carrier targeting counterpart and cargo. As a consequence, combined targeting resulted in a more homogenous, yet still specific and enhanced, delivery of ASM through different tissues, which is preferred in the case of diseases affecting multi-organ systems, such as Niemann-Pick disease A-B (Figure 6B).

Furthermore, in mice challenged with lipopolysaccharide, in order to induce inflammation typically associated with Niemann-Pick A-B disease and other maladies, dually-targeted anti-ICAM/TfR nanocarriers improved further ASM accumulation compared to a control situation (Figure 7). This pairs well with the fact that ICAM-1 is overexpressed under inflammatory conditions [36], and hence, dually-targeted nanocarriers retained the ability to respond to ICAM-1 overexpression. Interestingly, this phenomenon was observed to a much lesser extent in the case of the brain (*e.g.*, comparing the localization ratio and specificity index in Figure 7). This result is in accord with our previous observation indicating that TfR targeting seems to rule brain addressing (as opposed to the case of lungs) of dually-targeted anti-ICAM/TfR nanocarriers (Figure 5). Interestingly, this is despite the expected increase in

expression of ICAM-1, not TfR, in the brain under inflammatory conditions [55]. Hence, the resulting biodistribution of dually-targeted nanocarriers cannot be simply explained by their reduced valency to each individual receptor (as reported in the previous section), nor it corresponds to the combined biodistribution of their respective targeting moieties.

While we used a 50:50 ratio of two targeting antibodies on the nanocarrier surface, it is likely that further tuning of this parameter may improve organ selectivity. For example, selectivity for cancerous versus non-cancerous cells was enhanced by optimizing the ratio of folic acid and anti-EGFR antibody coupled to liposomes [52]. However, as indicated here, such optimization cannot be predicted, as numerous factors relative to both design parameter and physiological features may influence combined targeting strategies.

4. Conclusion

Combination targeting has recently arisen as a valuable tool to modulate biodistribution of drug delivery systems, where multi-targeted nanocarriers represent a new type of "ligand," with valency and size distinct from that of most natural counterparts. This approach may involve not only targeting to distinct cell-surface receptors, previously explored, but also different epitopes within a single receptor, shown here for the first time. Indeed, nanocarriers can critically affect *in vivo* targeting performance compared to free ligands (*e.g.*, antibodies) in an epitope-dependent manner. Presentation on the surface of nanocarriers decreased *in vivo* targeting specificity of anti-TfR-8D3, while the opposite effect was observed for anti-TfR-R17, and valency affected targeting by anti-TfR-8D3 nanocarriers more acutely than in the case of anti-TfR-R17 nanocarriers. Dually-targeted anti-TfR-R17/8D3 nanocarriers displayed a modified biodistribution compared to single-targeted counterparts, with intermediate targeting compared to parental formulations in lungs and liver, but not brain. Modified biodistribution was also observed for nanocarriers dually-targeted to distinct receptors, TfR and ICAM-1, where lung targeting was ruled by anti-ICAM counterpart, while anti-TfR defined brain targeting of anti-ICAM/TfR nanocarriers. Results obtained *in vivo* paired only partially with cell culture findings, highlighting the influence of physiological parameters, including cell and tissue type, receptor and epitope presence and accessibility, *etc.*, also indicating that these outcomes cannot be predicted using reductionist cell culture models. The effect of nanocarrier dual targeting in different organs resulted in modulation of the biodistribution of a therapeutic enzyme (ASM, deficient in a lysosomal storage disorder named Niemann-Pick disease A-B), both in control and disease-like conditions. Therefore, combination-targeting may aid the development of nanomedicines with biodistribution patterns tailored to better adapt to particular therapeutic needs.

Acknowledgments

This study was funded by a grant from the NIH (R01 HL098416) to S.Muro.

References

1. Allen TM, Cullis PR. Drug delivery systems: entering the mainstream. Science. 2004; 303:1818–1822. [PubMed: 15031496]
2. Torchilin VP. Drug targeting. Eur J Pharm Sci. 2000; 11(Suppl 2):S81–S91. [PubMed: 11033430]
3. Muro S, Koval M, Muzykantov V. Endothelial endocytic pathways: gates for vascular drug delivery. Curr Vasc Pharmacol. 2004; 2:281–299. [PubMed: 15320826]
4. Muro S. Strategies for delivery of therapeutics into the central nervous system for treatment of lysosomal storage disorders. Drug Deliv Transl Res. 2012; 2:169–186.

5. Chrastina A, Massey KA, Schnitzer JE. Overcoming in vivo barriers to targeted nanodelivery. Wiley Interdiscip Rev Nanomed Nanobiotechnol. 2011; 3:421–437. [PubMed: 21538941]
6. Muro S. Challenges in design and characterization of ligand-targeted drug delivery systems. J Control Release. 2012 In press.
7. Smith CW. 3. Adhesion molecules and receptors. J Allergy Clin Immunol. 2008; 121:S375–S379. quiz S414. [PubMed: 18241685]
8. Grove J, Marsh M. The cell biology of receptor-mediated virus entry. J Cell Biol. 195:1071–1082. [PubMed: 22123832]
9. Robbins GP, Saunders RL, Haun JB, Rawson J, Therien MJ, Hammer DA. Tunable leukopolymersomes that adhere specifically to inflammatory markers. Langmuir. 2010; 26:14089–14096. [PubMed: 20704280]
10. Gunawan RC, Almeda D, Auguste DT. Complementary targeting of liposomes to IL-1 alpha and TNF-alpha activated endothelial cells via the transient expression of VCAM-1 and E-selectin. Biomaterials. 2011; 32:9848–9853. [PubMed: 21944721]
11. Ferrante EA, Pickard JE, Rychak J, Klibanov A, Ley K. Dual targeting improves microbubble contrast agent adhesion to VCAM-1 and P-selectin under flow. J Control Release. 2009; 140:100–107. [PubMed: 19666063]
12. Eniola AO, Willcox PJ, Hammer DA. Interplay between rolling and firm adhesion elucidated with a cell-free system engineered with two distinct receptor-ligand pairs. Biophys J. 2003; 85:2720–2731. [PubMed: 14507735]
13. McAteer MA, Schneider JE, Ali ZA, Warrick N, Bursill CA, von zur Muhlen C, et al. Magnetic resonance imaging of endothelial adhesion molecules in mouse atherosclerosis using dualtargeted microparticles of iron oxide. Arterioscler Thromb Vasc Biol. 2008; 28:77–83. [PubMed: 17962629]
14. Weller GE, Villanueva FS, Tom EM, Wagner WR. Targeted ultrasound contrast agents: in vitro assessment of endothelial dysfunction and multi-targeting to ICAM-1 and sialyl lewisx. Biotechnol Bioeng. 2005; 92:780–788. [PubMed: 16121392]
15. Ying X, Wen H, Lu WL, Du J, Guo J, Tian W, et al. Dual-targeting daunorubicin liposomes improve the therapeutic efficacy of brain glioma in animals. J Control Release. 141:183–192. [PubMed: 19799948]
16. Zhang Y, Zhu C, Pardridge WM. Antisense gene therapy of brain cancer with an artificial virus gene delivery system. Mol Ther. 2002; 6:67–72. [PubMed: 12095305]
17. Chacko A-M, Nayak M, Greineder CF, Delisser HM, Muzykantov VR. Collaborative enhancement of antibody binding to distinct PECAM-1 epitopes modulates endothelial targeting. PloS one. 2012; 7:e34958. [PubMed: 22514693]
18. Garnacho C, Albelda SM, Muzykantov VR, Muro S. Differential intra-endothelial delivery of polymer nanocarriers targeted to distinct PECAM-1 epitopes. J Control Release. 2008; 130:226–233. [PubMed: 18606202]
19. Balyasnikova IV, Metzger R, Visintine DJ, Dimasius V, Sun ZL, Berestetskaya YV, et al. Selective rat lung endothelial targeting with a new set of monoclonal antibodies to angiotensin Iconverting enzyme. Pulm Pharmacol Ther. 2005; 18:251–267. [PubMed: 15777608]
20. Balyasnikova IV, Karran EH, Albrecht RF 2nd, Danilov SM. Epitope-specific antibodyinduced cleavage of angiotensin-converting enzyme from the cell surface. Biochem J. 2002; 362:585–595. [PubMed: 11879185]
21. Lee HJ, Engelhardt B, Lesley J, Bickel U, Pardridge WM. Targeting rat anti-mouse transferrin receptor monoclonal antibodies through blood-brain barrier in mouse. J Pharmacol Exp Ther. 2000; 292:1048–1052. [PubMed: 10688622]
22. Daniels TR, Bernabeu E, Rodriguez JA, Patel S, Kozman M, Chiappetta DA, et al. The transferrin receptor and the targeted delivery of therapeutic agents against cancer. Biochim Biophys Acta. 1820:291–317. [PubMed: 21851850]
23. Boado RJ, Zhang Y, Wang Y, Pardridge WM. Engineering and expression of a chimeric transferrin receptor monoclonal antibody for blood-brain barrier delivery in the mouse. Biotechnol Bioeng. 2009; 102:1251–1258. [PubMed: 18942151]

24. Zhou QH, Boado RJ, Lu JZ, Hui EK, Pardridge WM. Brain-penetrating IgG-iduronate 2-sulfatase fusion protein for the mouse. Drug Metab Dispos. 40:329–335. [PubMed: 22065691]
25. Ko YT, Bhattacharya R, Bickel U. Liposome encapsulated polyethylenimine/odn polyplexes for brain targeting. J Control Release. 2009; 133:230–237. [PubMed: 19013203]
26. van Rooy I, Mastrobattista E, Storm G, Hennink WE, Schiffelers RM. Comparison of five different targeting ligands to enhance accumulation of liposomes into the brain. J Control Release. 150:30–36. [PubMed: 21087646]
27. Hatakeyama H, Akita H, Maruyama K, Suhara T, Harashima H. Factors governing the in vivo tissue uptake of transferrin-coupled polyethylene glycol liposomes in vivo. Int J Pharm. 2004; 281:25–33. [PubMed: 15288340]
28. Bloemen PG, Henricks PA, van Bloois L, van den Tweel MC, Bloem AC, Nijkamp FP, et al. Adhesion molecules: A new target for immunoliposome-mediated drug delivery. FEBS Lett. 1995; 357:140–144. [PubMed: 7805880]
29. Weller GE, Lu E, Csikari MM, Klibanov AL, Fischer D, Wagner WR, et al. Ultrasound imaging of acute cardiac transplant rejection with microbubbles targeted to intercellular adhesion molecule-1. Circulation. 2003; 108:218–224. [PubMed: 12835214]
30. Chittasupho C, Xie SX, Baoum A, Yakovleva T, Siahaan TJ, Berkland CJ. ICAM-1 targeting of doxorubicin-loaded PLGA nanoparticles to lung epithelial cells. Eur J Pharm Sci. 2009; 37:141–150. [PubMed: 19429421]
31. Muro S, Wiewrodt R, Thomas A, Koniaris L, Albelda SM, Muzykantov VR, et al. A novel endocytic pathway induced by clustering endothelial ICAM-1 or PECAM-1. J Cell Sci. 2003; 116:1599–1609. [PubMed: 12640043]
32. Muro S, Garnacho C, Champion JA, Leferovich J, Gajewski C, Schuchman EH, et al. Control of endothelial targeting and intracellular delivery of therapeutic enzymes by modulating the size and shape of ICAM-1-targeted carriers. Mol Ther. 2008; 16:1450–1458. [PubMed: 18560419]
33. Jefferies WA, Brandon MR, Hunt SV, Williams AF, Gatter KC, Mason DY. Transferrin receptor on endothelium of brain capillaries. Nature. 1984; 312:162–163. [PubMed: 6095085]
34. Dautry-Varsat A. Receptor-mediated endocytosis: the intracellular journey of transferrin and its receptor. Biochimie. 1986; 68:375–381. [PubMed: 2874839]
35. Marlin SD, Springer TA. Purified intercellular adhesion molecule-1 (ICAM-1) is a ligand for lymphocyte function-associated antigen 1 (LFA-1). Cell. 1987; 51:813–819. [PubMed: 3315233]
36. Serrano, D.; Muro, S. Endothelial cell adhesion molecules and drug delivery applications. In: Aranda-Espinoza, H., editor. Mechanobiology of the endothelium. Maryland: Science Publishers; 2013. (under review)
37. Ghaffarian R, Bhowmick T, Muro S. Transport of nanocarriers across gastrointestinal epithelial cells by a new transcellular route induced by targeting ICAM-1. J Control Release. 2012; 163:25–33. [PubMed: 22698938]
38. He X, Miranda SR, Xiong X, Dagan A, Gatt S, Schuchman EH. Characterization of human acid sphingomyelinase purified from the media of overexpressing chinese hamster ovary cells. Biochim Biophys Acta. 1999; 1432:251–264. [PubMed: 10407147]
39. Papademetriou J, Garnacho C, Serrano D, Bhowmick T, Schuchman EH, Muro S. Comparative binding, endocytosis, and biodistribution of antibodies and antibody-coated carriers for targeted delivery of lysosomal enzymes to ICAM-1 versus transferrin receptor. J Inherit Metab Dis. 2012 In press.
40. Garlanda C, Parravicini C, Sironi M, De Rossi M, Wainstok de Calmanovici R, Carozzi F, et al. Progressive growth in immunodeficient mice and host cell recruitment by mouse endothelial cells transformed by polyoma middle-sized T antigen: implications for the pathogenesis of opportunistic vascular tumors. Proc Natl Acad Sci U S A. 1994; 91:7291–7295. [PubMed: 8041783]
41. Hsu J, Serrano D, Bhowmick T, Kumar K, Shen Y, Kuo YC, et al. Enhanced endothelial delivery and biochemical effects of alpha-galactosidase by ICAM-1-targeted nanocarriers for fabry disease. J Control Release. 2011; 149:323–331. [PubMed: 21047542]
42. Bjorn MJ, Groetsema G. Immunotoxins to the murine transferrin receptor: intracavitary therapy of mice bearing syngeneic peritoneal tumors. Cancer Res. 1987; 47:6639–6645. [PubMed: 3499979]

43. Panaccio M, Zalcberg JR, Thompson CH, Leyden MJ, Sullivan JR, Lichtenstein M, et al. Heterogeneity of the human transferrin receptor and use of anti-transferrin receptor antibodies to detect tumours in vivo. Immunol Cell Biol. 1987; 65(Pt 6):461–472. [PubMed: 2452131]
44. Takahashi S, Esserman L, Levy R. An epitope on the transferrin receptor preferentially exposed during tumor progression in human lymphoma is close to the ligand binding site. Blood. 1991; 77:826–832. [PubMed: 1704266]
45. van Driel IR, Goding JW. Heterogeneous glycosylation of murine transferrin receptor subunits. Eur J Biochem. 1985; 149:543–548. [PubMed: 2988950]
46. Muro S, Dziubla T, Qiu W, Leferovich J, Cui X, Berk E, et al. Endothelial targeting of highaffinity multivalent polymer nanocarriers directed to intercellular adhesion molecule 1. J Pharmacol Exp Ther. 2006; 317:1161–1169. [PubMed: 16505161]
47. Grill J, Van Beusechem VW, Van Der Valk P, Dirven CM, Leonhart A, Pherai DS, et al. Combined targeting of adenoviruses to integrins and epidermal growth factor receptors increases gene transfer into primary glioma cells and spheroids. Clin Cancer Res. 2001; 7:641–650. [PubMed: 11297260]
48. Willmann JK, Lutz AM, Paulmurugan R, Patel MR, Chu P, Rosenberg J, et al. Dual-targeted contrast agent for us assessment of tumor angiogenesis in vivo. Radiology. 2008; 248:936–944. [PubMed: 18710985]
49. Xu Q, Liu Y, Su S, Li W, Chen C, Wu Y. Anti-tumor activity of paclitaxel through dualtargeting carrier of cyclic rgd and transferrin conjugated hyperbranched copolymer nanoparticles. Biomaterials. 33:1627–1639. [PubMed: 22118775]
50. Yan H, Wang L, Wang J, Weng X, Lei H, Wang X, et al. Two-order targeted brain tumor imaging by using an optical/paramagnetic nanoprobe across the blood brain barrier. ACS Nano. 6:410–420. [PubMed: 22148835]
51. Markoutsa E, Papadia K, Clemente C, Flores O, Antimisiaris SG. Anti-Aβ-MAb and dually decorated nanoliposomes: effect of Aβ1-42 peptides on interaction with hCMEC/D3 cells. Eur J Pharm Biopharm. 81:49–56. [PubMed: 22386910]
52. Saul JM, Annapragada AV, Bellamkonda RV. A dual-ligand approach for enhancing targeting selectivity of therapeutic nanocarriers. J Control Release. 2006; 114:277–287. [PubMed: 16904220]
53. Li X, Zhou H, Yang L, Du G, Pai-Panandiker AS, Huang X, et al. Enhancement of cell recognition in vitro by dual-ligand cancer targeting gold nanoparticles. Biomaterials. 32:2540–2545. [PubMed: 21232787]
54. Garnacho C, Dhami R, Simone E, Dziubla T, Leferovich J, Schuchman EH, et al. Delivery of acid sphingomyelinase in normal and Niemann-Pick disease mice using intercellular adhesion molecule-1-targeted polymer nanocarriers. J Pharmacol Exp Ther. 2008; 325:400–408. [PubMed: 18287213]
55. Henninger DD, Panes J, Eppihimer M, Russell J, Gerritsen M, Anderson DC, et al. Cytokineinduced VCAM-1 and ICAM-1 expression in different organs of the mouse. J Immunol. 1997; 158:1825–1832. [PubMed: 9029122]

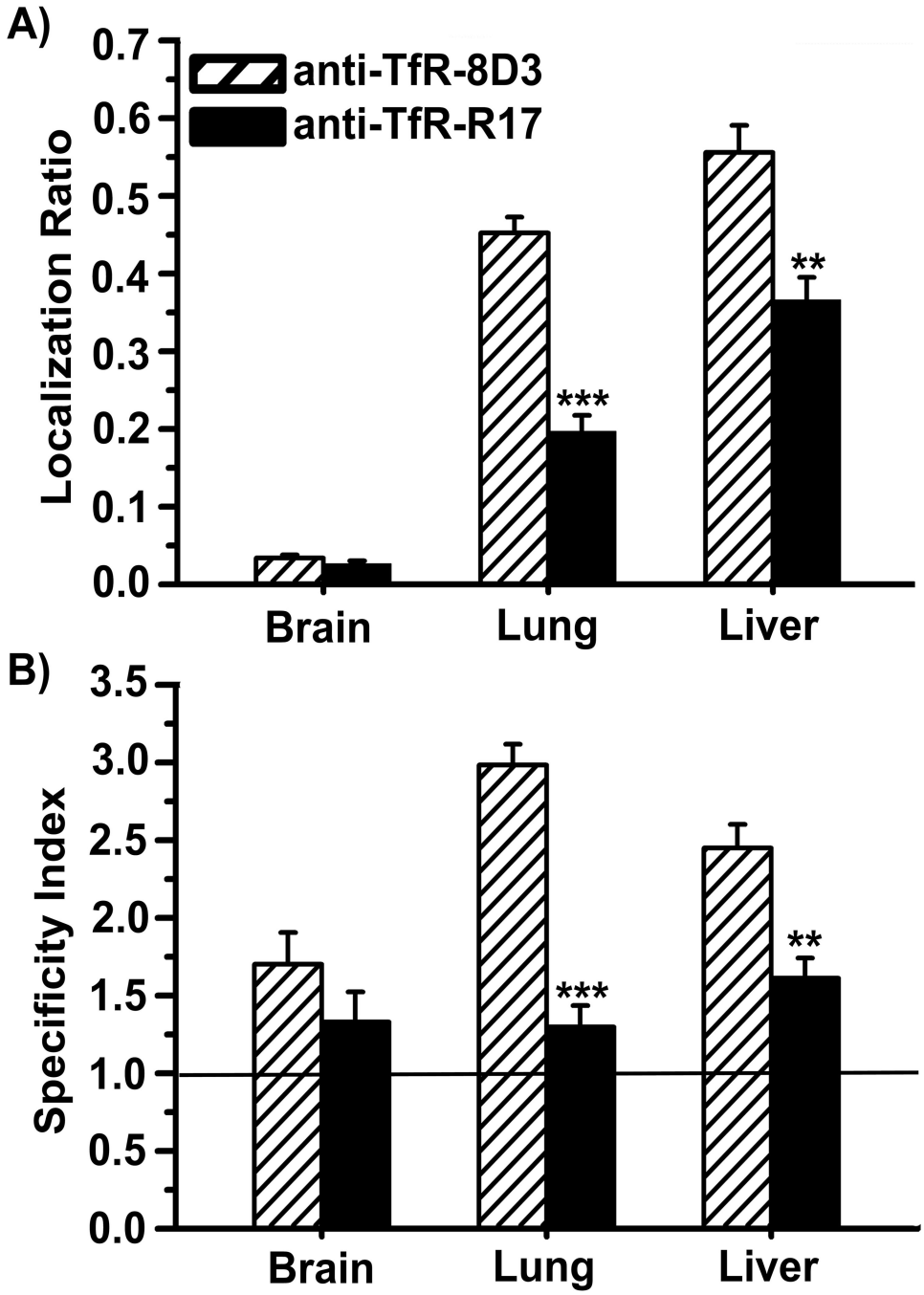

Figure 1.

Biodistribution of free anti-TfR-8D3 vs. anti-TfR-R17 in mice. The localization ratio or LR (A) and specificity index or SI (B) in brain, lungs, and liver were calculated as described (see methods). Data are mean ± S.E.M. ($n \geq 3$ mice). ** $p < 0.01$; *** $p < 0.001$, comparing anti-TfR-8D3 to anti-TfR-R17, by Student's *t*-test.

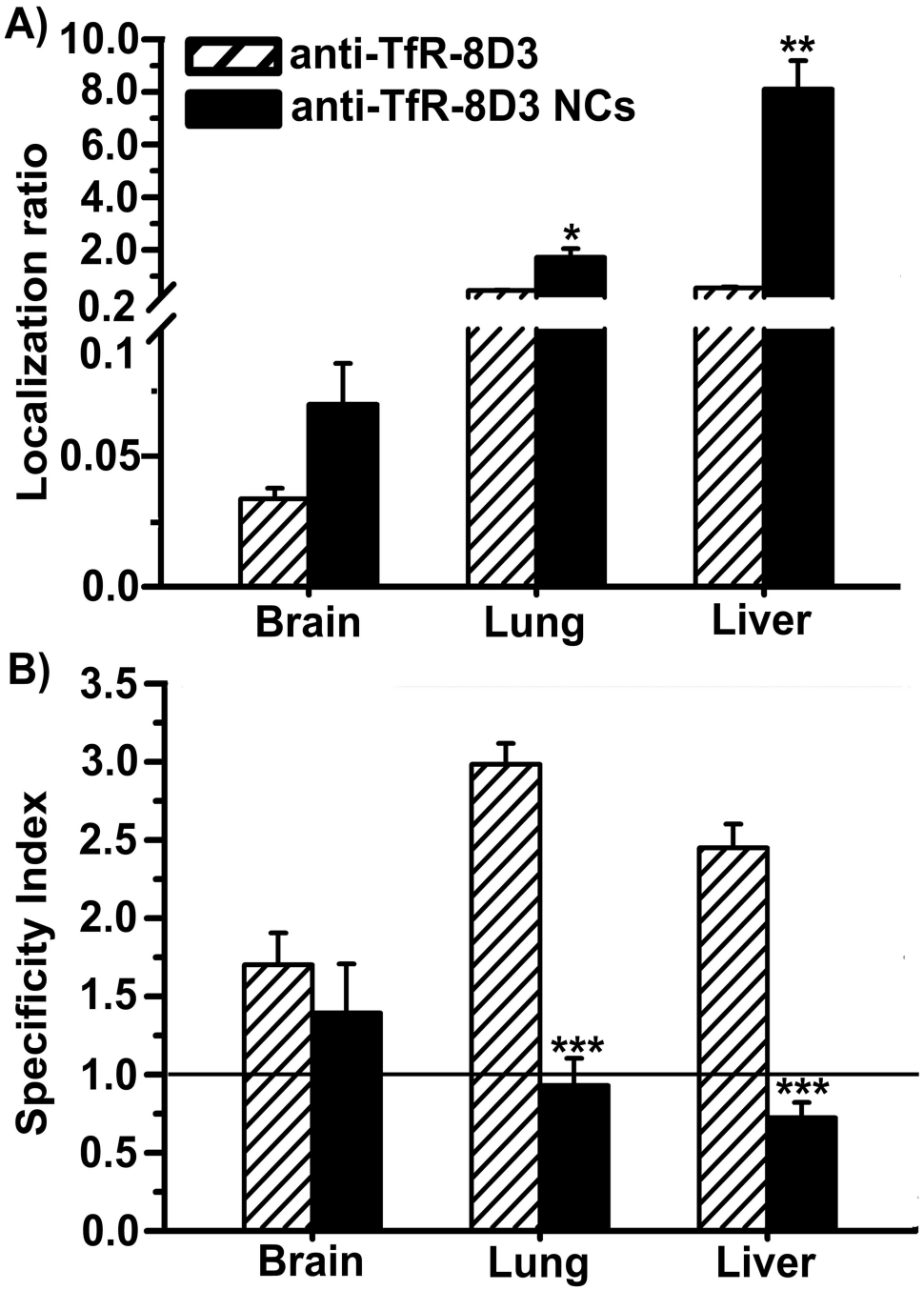

Figure 2.

Biodistribution of free anti-TfR-8D3 vs. nanocarriers coated with anti-TfR-8D3. Localization ratio (LR) and specificity index (SI) of brain, lungs, and liver are shown in (A) and (B), respectively. Data are mean ± S.E.M. ($n \geq 3$ mice). * $p < 0.05$; ** $p < 0.01$; *** $p < 0.001$, comparing anti-TfR-8D3 to anti-TfR-8D3 NCs, by Student's *t*-test. NCs = nanocarriers.

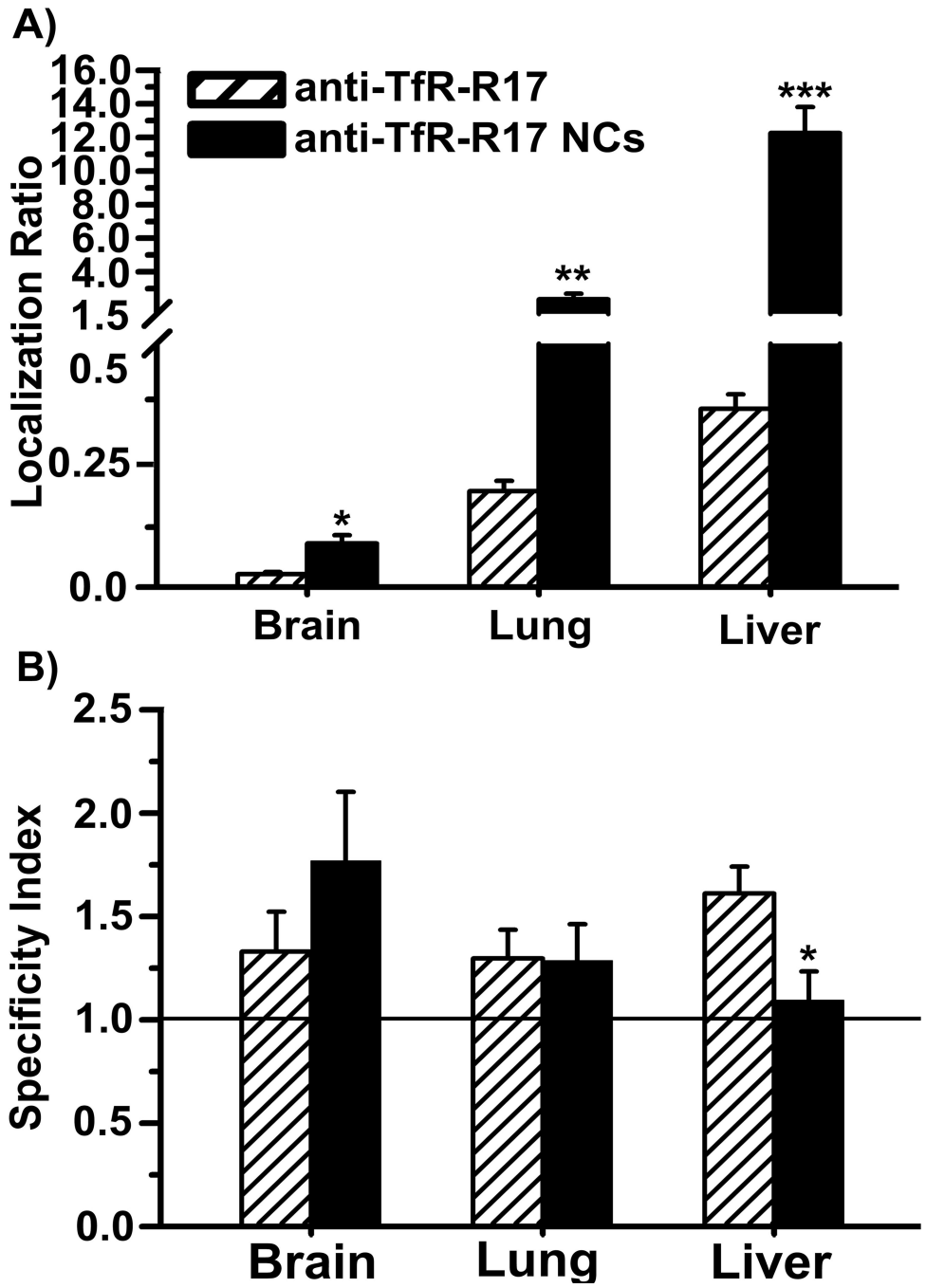

Figure 3.

Biodistribution of free anti-TfR-R17 vs. nanocarriers coated with anti-TfR-R17. Localization ratio (LR) and specificity index (SI) of brain, lungs, and liver are shown in (A) and (B), respectively. Data are mean ± S.E.M. ($n \geq 3$ mice). * $p < 0.05$; ** $p < 0.01$, *** $p < 0.001$, comparing anti-TfR-R17 to anti-TfR-R17 NCs, by Student's *t*-test. NCs = nanocarriers.

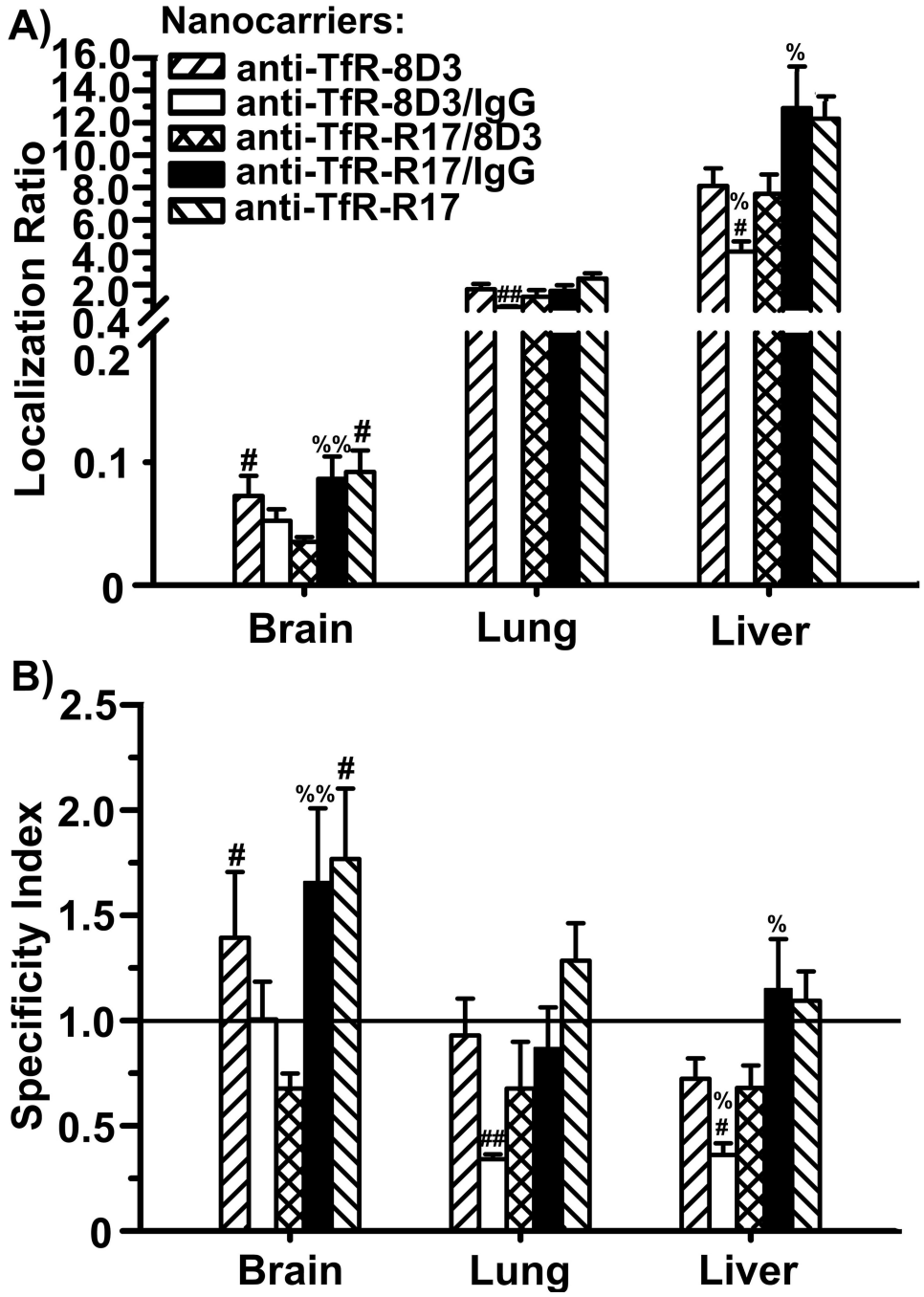

Figure 4.

Biodistribution of nanocarriers coated with both anti-TfR-8D3 and anti-TfR-R17. Localization ratio (LR) and specificity index (SI) of brain, lungs, and liver are shown in (A) and (B), respectively. Data are mean ± S.E.M. ($n \geq 3$ mice).* compares anti-TfR-R17 NCs to anti-TfR-8D3 NCs; # compares dually-coated nanocarriers (either Ab/IgG or Ab1/Ab2) to their respective parental, single-targeted nanocarriers; % compares anti-TfR-R17/8D3 NCs to control Ab/IgG NCs. *,#,%, $p < 0.05$; **,##,%%, $p < 0.01$; ***,###,%%%, $p < 0.001$, by Student's *t*-test. NCs = nanocarriers.

Ab = antibody.

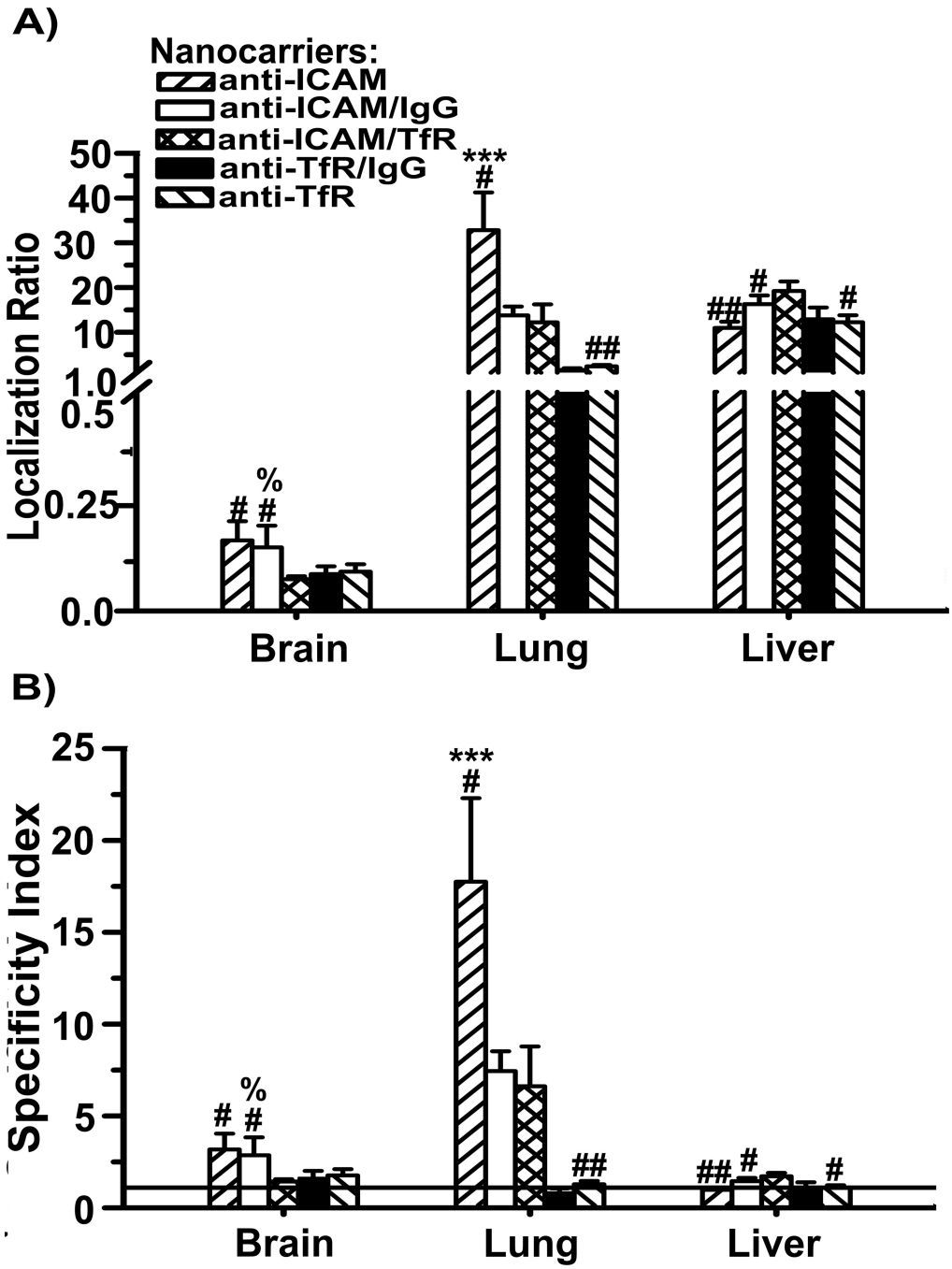

Figure 5.

Biodistribution of nanocarriers coated with anti-ICAM-1 and anti-TfR in mice. Localization ratio (LR) and specificity index (SI) of brain, lungs, and liver are shown in (A) and (B), respectively. Data are mean ± S.E.M. ($n \geq 3$ mice). * compares anti-TfR NCs to anti-ICAM NCs; # compares dually-coated nanocarriers (either Ab/IgG or Ab1/Ab2) to their respective parental, single-targeted nanocarriers; % compares anti-ICAM/anti-TfR NCs to control Ab/IgG NCs. *,#,%, $p < 0.05$; **,##,%%, $p < 0.01$; ***,###,%%%, $p < 0.001$, by Student's *t*-test. NCs = nanocarriers.

Ab = antibody.

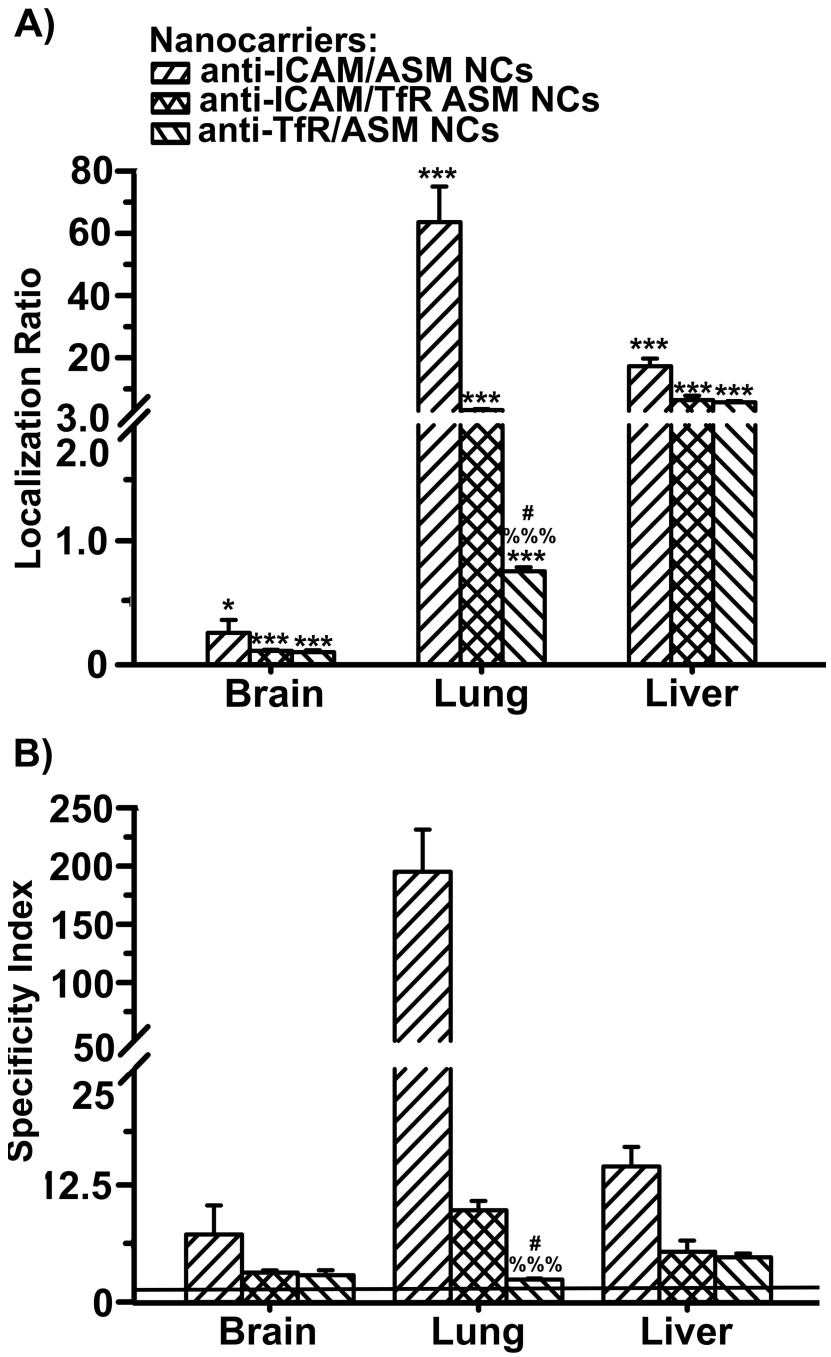

Figure 6.

Delivery of ASM by nanocarriers targeted to both ICAM-1 and TfR. Localization ratio (LR) and specificity index (SI) of brain, liver, and lungs are shown in (A) and (B), respectively. Data are mean ± S.E.M. ($n = 3$). * Compares enzyme vs nanocarrier-coupled enzyme for each target; # compares targeting between single-targeted nanocarriers; % compares targeting of dually-targeted nanocarriers vs. single-targeted counterparts. *,#,% $p < 0.05$; **,##,%% $p < 0.01$; ***,###,%%% $p < 0.001$ by Student's *t*-test.

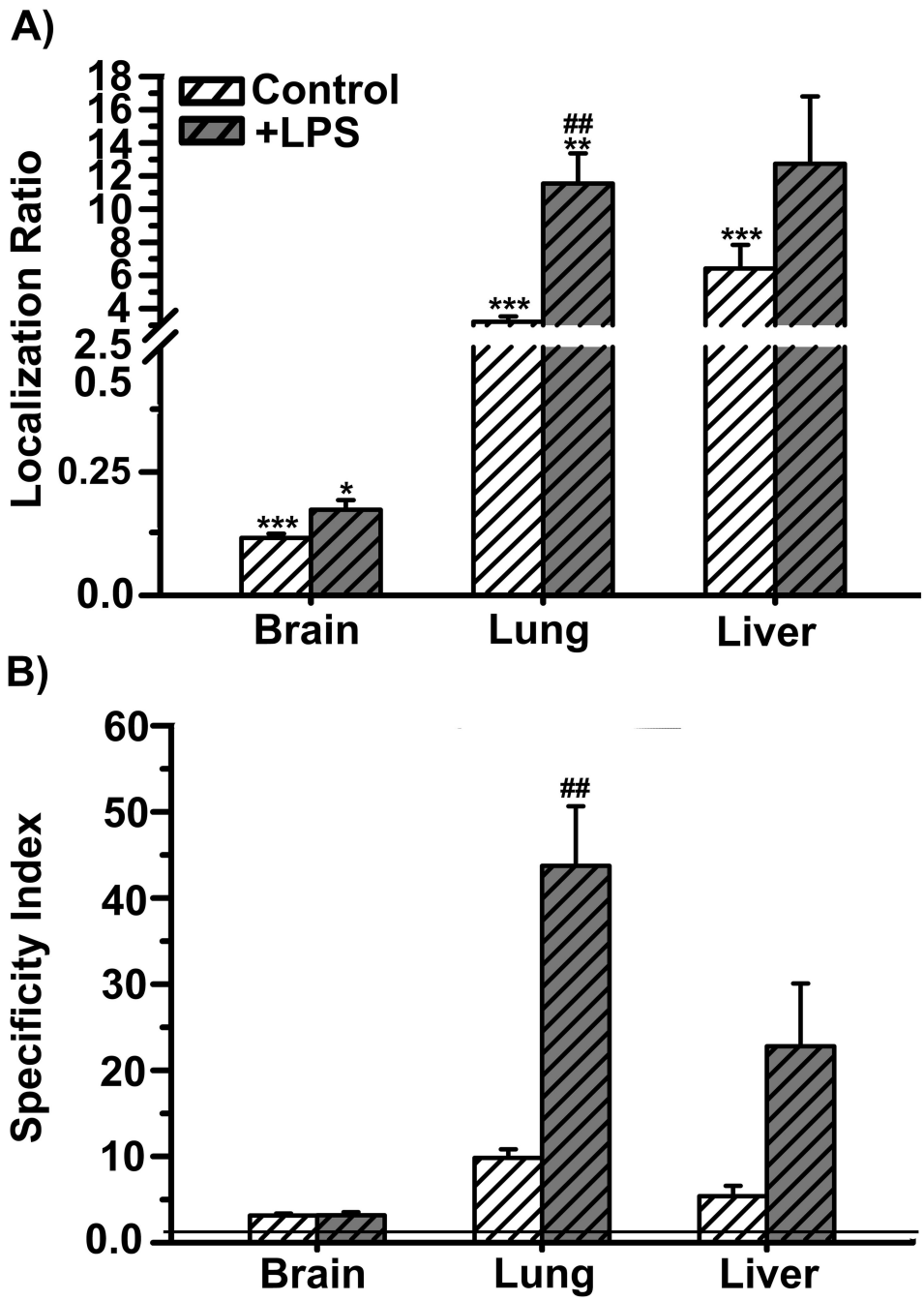

Figure 7.

Inflammation and ASM delivery by nanocarriers coated with anti-ICAM-1 and anti-TfR. Localization ratio (LR) and specificity index (SI) of brain, lungs, and liver are shown in (A) and (B), respectively. Data are mean ± S.E.M. ($n \geq 3$ mice). * compares free enzyme vs enzyme coupled to nanocarriers coated with both anti-ICAM and anti-TfR; # compares control mice vs mice pre-treated with lipopolysaccharide (LPS). *,# $p < 0.05$; **,## $p < 0.01$; ***,### $p < 0.001$, by Student's *t*-test.

Table 1

Nanocarrier	Size (nm)	Zeta potential (mv)	Antibodies per nanocarrier		Nanocarriers bound per cell[a]
Single Targeting:					
Anti-ICAM	219±4.54	−9.37±0.47	273±37.0		49.9±9.80
Anti-TfR-8D3	265±27.9	−14.5±3.4	185±2.37		31.6±2.28
Anti-TfR-R17	235±15.1	−15.9±1.63	220±6.27		3.71±0.61
Combined Targeting:					
Anti-TfR-R17/8D3	258±12.2	−14.5±3.67	8D3: 115±0.94	R17: 140±7.22	11.9±0.76
Anti-TfR-R17/IgG	251±13.2	−9.50±0.28	R17: 154±0.87	IgG: 136±0.31	6.72±1.63
Anti-TfR-8D3/IgG	255±40.0	−12.9±3.89	8D3: 98.5±4.02	IgG: 152±9.74	14.7±1.16
Anti-ICAM/anti-TfR (clone R17)	216±11.1	−11.6±0.14	Anti-ICAM: 132±12.4	Anti-TfR: 145±9.72	21.0±4.12
Anti-ICAM/IgG	240±17.9	−9.02±0.34	Anti-ICAM: 124±24.5	IgG 139±2.41	16.6±2.50

Data are Mean ± S.E.M.; Ab = antibody; N/A = not applicable;

[a] $p<0.05$ compared to control IgG NCs, in all cases (by Student's *t*-test).